Ann. For. Res. 66(2): 101-120, 2023
https://doi.org/10.15287/afr.2023.3361

ANNALS OF FOREST RESEARCH
www.afrjournal.org

Stratification of vertical canopy structure to improve estimation of forest inventory attributes using airborne LiDAR data in a large subtropical region of China

Mei Zhou[1], Chungan Li[2]✉, Zhen Li[3], Zhu Yu[3], Xiangbei Zhou[4]

Zhou M., Li C., Li Z., Yu Z., Zhou X., 2023. Stratification of vertical canopy structure to improve estimation of forest inventory attributes using airborne LiDAR data in a large subtropical region of China. Ann. For. Res. 66(2): 101-120.

Abstract Over the last two decades, airborne light detection and ranging (LiDAR) has been developed into an advanced tool for practical forest resource inventory monitoring over large areas. Nonetheless, improving the accuracy of forest inventory attribute estimations remains an ongoing challenge. This paper introduces a novel framework for estimating forest inventory attributes based on the stratification of vertical forest structures (VFS). According to the composition and spatial arrangement of the superior, middle, and inferior strata in the tree layer, the forest stand was classified into six distinct VFS classes. Subsequently, the multiplicative power models were established for the stratification-based estimations of the forest inventory attributes, including stand volume (VOL), basal area (BA), and above-ground biomass (AGB), by using a rule-based exhaustive combination approach, and their performances were comparatively analyzed. The result indicated that: compared to the accuracy (relative root mean squared error, rRMSE) of the species-based estimation, the weighted average rRMSE of stratum-based VOL, BA, and AGB estimations of four forest types (Chinese fir, Masson pine, eucalyptus, and broadleaf forests) decreased by 0.3%–7.3%, +3.6%–9.4%, and 0.7%–8.7%, respectively, and the accuracy was significantly improved after stratification. Even after clustering the VFS into two or three classes using cluster analysis, the accuracy of forest attribute estimations remained superior to that of the species-based estimations. Notably, the coefficients of variation for both forest attributes and LiDAR metrics experienced a substantial decrease, and their statistical relationship considerably strengthened within most strata post-VFS classification, which led to an improvement in the accuracy of the forest attribute estimations. The methodology presented in this paper provides a significant advance in improving the accuracy of forest inventory attributes for large areas using airborne LiDAR data.

Keywords: vertical forest structure; stratification; area-based approach; multiplicative power model; accuracy.

Addresses: [1]School of Computer, Electronic and Information, Guangxi University, Nanning, China.| [2]Forestry College of Guangxi University, Nanning, China.| [3] Guangxi Forest Inventory and Planning Institute, Nanning, China.| [4] Guangxi Natural Resources Vocational and Technical College, Fushui, China.

✉ **Corresponding Author:** Chungan Li (chungan@gxu.edu.cn).

Manuscript: received December 9, 2023; revised December 29, 2023; accepted December 29, 2023.

Introduction

Airborne laser scanning (ALS, also referred to as light detection and ranging, LiDAR) is an active remote sensing technology that accurately depicts the three-dimensional (3D) structure of forest canopies (Montaghi et al. 2013, Bouvier et al. 2015). Robust statistical relationships exist between certain descriptive statistics of ALS data (LiDAR-derived metrics) and field-measured attributes (Næsset et al. 2004, Gobakken et al. 2012, Wulder et al. 2012), making it widely used for estimating and mapping forest attributes like tree height (H), diameter at breast height (DBH), basal area (BA), stand volume (VOL), above-ground biomass (AGB), carbon, and leaf area index (LAI) (Nilsson, 1996, Means et al. 2000, Lefsky et al. 2002, Næsset and Økland 2002, Ioki et al. 2010, Tang et al. 2015, Marczak et al. 2020, Leboeuf et al. 2022). Since 2002, ALS has replaced conventional field measurement in Scandinavian countries (Næsset et al. 2004) and Canada (White et al. 2017) for operational forest resource inventory. It is also widely used in large-scale plantations and ecological monitoring (Watt & Watt, 2013, Matasci et al. 2018, Silva et al. 2017a, b). However, improving the accuracy of forest attributes estimation using airborne LiDAR remains a tireless pursuit for foresters and researchers, posing a significant challenge for airborne LiDAR forest applications.

Different forest types consist of diverse tree species, each with unique biological and ecological characteristics that result in variations in height, canopy shape (Gökkaya et al. 2015), spatial arrangement of canopy layers (Zolkos et al. 2013), canopy material distribution (Nelson et al. 2007), allometric equation for calculating forest attributes (Zhao et al. 2012), and wood carbon density (van Leeuwen et al. 2011). The relationships between the LiDAR metrics and forest attributes often vary among forest types and tree species (Hauglin et al. 2021). Hence, airborne LiDAR-based forest attribute estimations typically require stratification. While some studies lack sufficient field plots for stratification (e.g., Knapp et al. 2020, Fekety et al. 2015, Fassnacht et al. 2014, Asner et al. 2012, Palace et al. 2015, Luo et al. 2018, Song et al. 2016, Chirici et al. 2016, Laurin et al. 2016, González-Jaramillo et al. 2018), most utilize stratifications based on forest type (e.g., deciduous, coniferous, and mixed forests) (Viana et al. 2012, Nord-Larsen & Schumacher 2012, Singh et al. 2015, Latifi et al. 2015, Nelson et al. 2017, Zhang et al. 2017, Bouvier et al. 2015, Chen et al. 2022), or dominant tree species (Chen et al. 2012, Keränen et al. 2016, Maltamo et al. 2016, Bohlin et al. 2017, Yang et al. 2021, Novo-Fernández et al. 2019, Hill et al. 2018, Jiang et al. 2020). Nordic countries commonly employ tree species, site productivity, or development classes for stratification (Næsset, 2004, Gobakken & Næsset, 2008, Gobakken et al. 2013, McRoberts et al. 2015, Gobakken et al. 2012, de Lera Garrido et al. 2020, Hauglin et al. 2021). Additionally, some studies stratify forests based on LiDAR data, such as the 90th height percentile and the proportion of ground echoes vs. canopy echoes (VEG) (Maltamo et al. 2011), the L-coefficient of variation of LiDAR echo heights (*L*cv; equivalent to the Gini coefficient, GCH) (Adnan et al. 2021), and the relationships between canopy height and above-ground biomass (Jiang et al. 2020). Numerous studies have shown that: (1) proper stratification could improve the accuracy of forest attribute estimations (Chen et al. 2022), reduce the effect of under- and over-estimation problems (Jiang et al. 2020); (2) the finer the forest stratification, the higher the accuracy of forest attribute estimation. A study demonstrated that stratification by dominant tree species was superior to stratification by forest types (e.g., coniferous and broadleaf forests) (Chen et al. 2022), while Hauglin et al. (2021) found that stratification by species and maturity class (e.g., young and mature forests) had lower root mean squared error (RMSE) than stratification by main tree species groups (e.g., spruce, pine, and deciduous); (3) ALS data as *a priori* information to select field training plots provided better estimation (Maltamo et al. 2011); and (4) proper stratification may reduce the number of sample plots needed (Jiang et al. 2020, Hauglin et al. 2021). Forest stands of the same forest type or dominant species, or even of the same age class, have single-, double-, and multi-storied forests, so their vertical canopy structures vary widely. Even for the single-storied stands, there are both pruned and unpruned stands, and their 3D structures also vary considerably. Although some scholars have used LiDAR variables to classify vertical structure, the classification results lack clear ecological significance (Adnan et al. 2021). Consequently, stratifying the vertical forest structures and conducting stratification-based estimation with airborne LiDAR data can potentially improve the accuracy of forest attribute estimation.

Recently, Zhou and Li (2023) proposed a novel approach for automated mapping of the vertical forest structure (VFS) in a large subtropical region based on discrete airborne LiDAR data. Their proposed approach exhibits high accuracy and generalization across forest types, species, and study sites, demonstrating its ecological and forestry significance. Building on Zhou and Li's work, the overall scientific aim of this study is to develop a new framework for airborne LiDAR forest inventory attribute estimation, utilizing an area-based method and vertical structure stratification of forest stands. This research aims to (1) investigate the effect of VFS stratification on the accuracy of forest attribute estimations, and (2) reveal the mechanism for improving the accuracy of forest attribute estimations using VFS stratification based on airborne LiDAR data. The authors anticipate that their approach will further improve the accuracy of forest attribute estimation over large areas using airborne LiDAR data.

Materials and Methods

Study area

The study area encompasses the entire Guangxi Zhuang Autonomous Region, China, with geographical coordinates ranging from 104°28′ to 112°04′E and 20°54′ to 26°24′N, covering an area of 237.6 × 10^3 km^2 (Fig. 1).

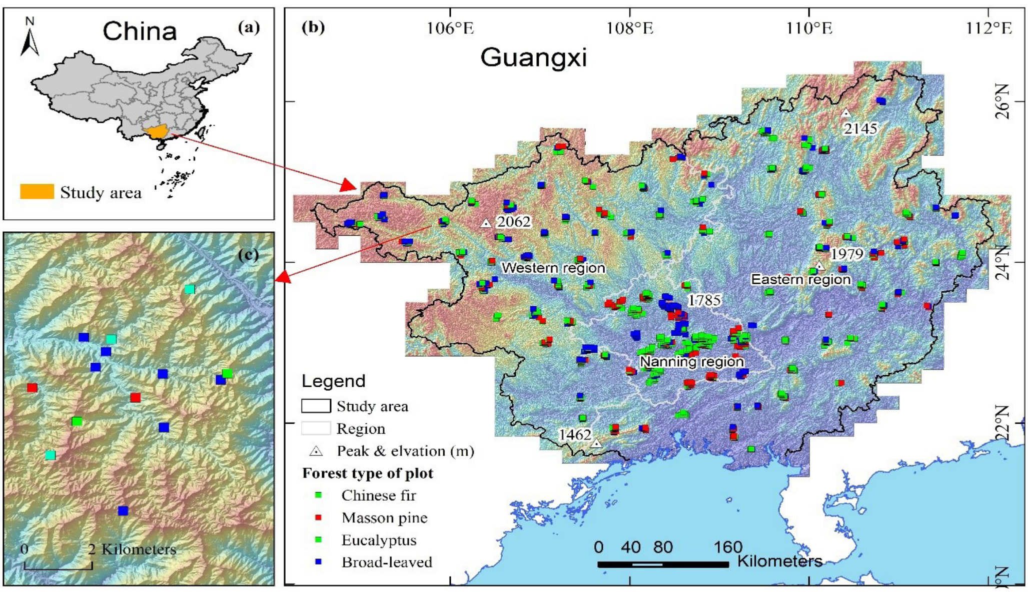

Figure 1 Study area and distribution of the field plots. (a) geographic location of the study area in China; (b) distribution of plot-clusters in three regions in the study area; and (c) locations of field plots in a cluster.

The study area was divided into three regions according to the financial allocation, namely the Nanning, eastern, and western regions. For further insights into the study area's specific characteristics, additional details can be found in the works of Li et al. (2022) and Zhou and Li (2023).

Field data and LiDAR data

The field plots in the Nanning, eastern, and western regions were measured from October 2016 to January 2017, November 2018 to May 2019, and August 2019 to January 2020, respectively. The forests in the study area were categorized into four types according to the dominant tree species and species groups, namely Chinese fir (*Cunninghamia lanceolate* (Lamb.) Hook) forest, Masson pine (approximately 90% is *Pinus massoniana* Lamb., with the remainder being *P. elliottii* Engelmann and *P. yunnanensis* Franch) forest, eucalyptus (mainly *Eucalyptus urophylla* S. T. Blake and *E. grandis* × *urophylla*) forest plantation, and broad-leaved (includes a large number of tree species) forest. A total of 1003 rectangular plots with a size of 30 m × 20 m were distributed in clusters over the study area, and each was subdivided into four sub-plots with an area of 15 m × 10 m.

All live trees with a DBH (1.3 m above the ground) ≥ 5 cm within the sub-plot were measured and recorded. Tree height was measured using a Haglöf Vertex IV hypsometer (Haglöf, Långsele, Västernorrland, Sweden) for three average trees and the tallest tree in each subplot. The VOL was calculated using provincial species-specific allometric equations (Liao & Huang 1986), using BA and mean height as predictors. The AGB of an individual tree was calculated using species-specific allometric equations (Cai et al. 2018), using DBH as the predictor. Table 1 provides the summary statistics for the 1003 field plots. Comprehensive details regarding plot installation, configuration, measurement procedures, and positioning are provided in the works of Li et al. (2023) and Zhou and Li (2023).

Table 1 Summary statistics for measured field plots data. CV is the coefficient of variation.

Forest type	Sample size	Stem density ($stem \cdot ha^{-1}$)	Stand Volume (VOL)		Basal Area (BA)		Above ground biomass (AGB)	
			Mean ($m^3 \cdot ha^{-1}$)	CV (%)	Mean ($m^2 \cdot ha^{-1}$)	CV (%)	Mean ($Mg \cdot ha^{-1}$)	CV (%)
Chinese fir	222	683-6883	193.60	46.58	31.91	29.34	86.97	35.35
Masson pine	260	350-3917	192.03	46.94	27.95	31.71	114.33	35.70
Eucalyptus	269	517-3350	141.91	17.24	17.24	34.12	78.25	45.47
Broad-leaved	252	233-4800	111.80	19.62	19.64	41.07	90.60	48.25

LiDAR data were acquired separately in the Nanning, eastern, and western regions from October 2016 to April 2017, October 2018 to October 2019, and August 2019 to January 2020, respectively. The Riegl VQ-1560 and Riegl VQ-1560i laser scanning systems from Riegl Laser Measurement Systems GmbH in Horn, Austria, were used to collect LiDAR data in all three regions. The final average point density was 5.54 (±2.14) points·m^2. The LiDAR survey flight, sensor parameters, and preprocessing method of point clouds were described in detail in the works of Li et al. (2023) and Zhou and Li (2023).

Classification and clustering of the vertical forest structure

Zhou and Li (2023) presented a procedure for mapping the VFS using discrete airborne LiDAR data. The fundamental methodology and steps of the procedure are summarized below.

(1) The tree layer was stratified into three strata: superior (T_1), middle (T_2), and inferior (T_3), following the stand dominance height criteria of the International Union of Forestry Research Organizations (IUFRO) (Neto et al. 2018). In this approach, the 99th height percentile (*hp*99) of LiDAR point clouds was used to replace the stand dominance height. Based on the composition and spatial arrangement of the three tree strata, the VFS

of the tree layer was further classified into six classes, as visually presented in Fig. 2.

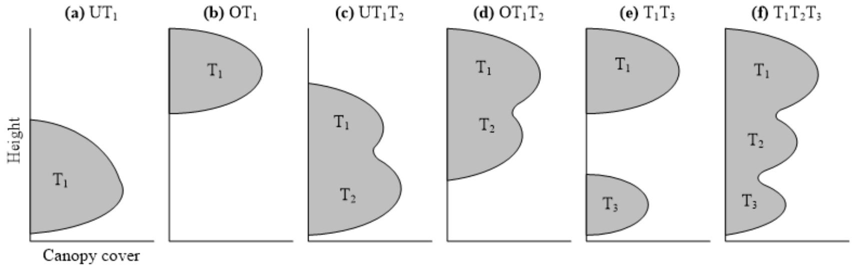

Figure 2 Stratification of the VFS of tree layers based on the composition and spatial arrangement of the three strata (Zhou & Li 2023).

(2) The study area was subdivided into an array of grid cells, with each grid cell matching the size of a field plot. LiDAR point clouds enclosed in the field plots and grid cells were segmented into 100 height bins, covering the range from the top to the ground. Each height bin was assigned a value representing the proportion of the number of returns enclosed in that bin to the total number of returns of all echoes within the field plot or grid cell. This process generated a height-frequency histogram.

(3) A univariate ten-order polynomial was used to fit the height-frequency histogram, creating the vertical canopy profiles, also known as pseudo-waveforms.

(4) A comprehensive set of vertical structure parameters was then extracted from the pseudo-waveforms. These parameters characterized the vertical canopy structures, including the surface height of the profile layer (h_{ls}), height to the base of the profile layer (h_{lb}), layer length of the profile layer (h_{la}), layer ratio of the profile layer (*LR*), canopy surface height (h_{cs}), height to the base of the canopy (h_{cb}), canopy length (h_{cl}), and canopy ratio (*CR*), cover of the superior (C_{T_1}), middle (C_{T_2}), and inferior (C_{T_3}) layers, etc.

(5) According to the number of effective peaks of the pseudo-waveforms and a selection of vertical structure parameters, a total of 43 model profiles were selected from the field plot. These profiles were used to develop 43 classification rules using the vertical structure parameters to classify and map the VFS of the field plot or study area into six classes.

Visual interpretation of the pseudo-waveforms and vertical profiles of the point clouds were employed to identify the VFS classes in the field plots, and these results served as a reference for validating the classification. The overall accuracy of the tree layer classification in the 1147 field plots (including 144 field plots in rocky mountain forests) was 95.5%, with a Kappa coefficient of 0.936. It should be noted that in the study of Zhou and Li (2023), the forest canopy was divided into the tree, shrub, and herbaceous layers, which were further classified into 24 VFS classes, with an overall accuracy of 94.7% and a Kappa coefficient of 0.937. In an area of 811,000 ha, 99.8% of the grid cells were successfully mapped for vertical forest structures.

As some classes had fewer than 20 field plots and were unsuitable for estimating forest inventory attributes, they were grouped into similar classes. Consequently, three, four, three, and five VFS classes were identified in the field plot of Chinese fir, Masson pine, eucalyptus, and broad-leaved forests, respectively. While estimating forest inventory attributes by stratum, the more strata there are, the more field plots are needed. To explore the feasibility of reducing the VFS number and effectively minimizing the sample size in the stratification-based estimation of forest inventory attributes, classes with similar vertical structures were clustered. The coefficient of variation of the height distribution of LiDAR point clouds (Hcv) represents the variation in the height distribution of the laser point clouds, while the canopy ratio (*CR*, equal to the canopy height (length) divided by the canopy surface height) characterizes the canopy shape. Both *H*cv and *CR* serve as indicators of the differences in the vertical structure of the canopy. Statistical analysis of the field plots revealed that *Hcv* and *CR* effectively characterized the differences among the vertical structure classes (Table 2).

Table 2 Number of the vertical forest structure classes and their mean *Hcv* and *CR* in the field plots.

Forest type	Par	(1) UT_1	(2) OT_1	(3) UT_1T_2	(4) OT_1T_2	(5) T_1T_3	(6) $T_1T_2T_3$
Chinese	No	53	108		61		
fir	*H*cv	0.30	0.19		0.27		
	CR	0.78	0.55		0.73		
Masson	No	38	149		36		37
pine	*H*cv	0.33	0.22		0.30		0.37
	CR	0.79	0.49		0.73		0.81
Eucalyptus	No		212		30	27	
	*H*cv		0.21		0.31	0.42	
	CR		0.39		0.70	0.62	
Broad-	No	43	42	40	80		47
leaved	*H*cv	0.32	0.23	0.36	0.28		0.38
	CR	0.79	0.56	0.85	0.72		0.85

Note: Par: parameter; No: Number of plots

Using the systematic clustering analysis, the vertical structures for all forest types were ultimately grouped into two or three classes based on *H*cv and *CR* (Fig. 3).

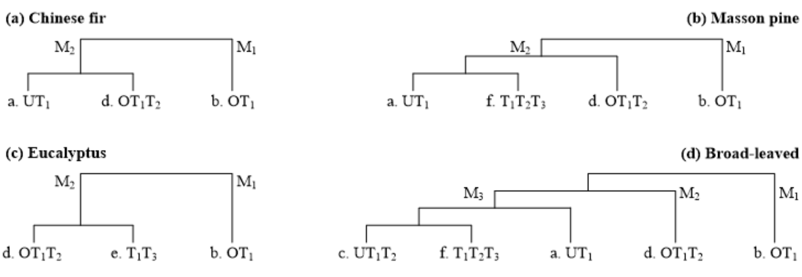

Figure 3 Dendrogram for classifying the vertical forest structures into two or three clusters: (a) Chinese fir; (b) Masson pine; (c) eucalyptus, and (d) broad-leaved forest.

Model calibration and validation

Over the past two decades, numerous studies have been conducted on various forest types and forest attributes (e.g., H, DBH, BA, VOL, AGB, etc.), resulting in various estimation models (Zolkos et al. 2013; Latifi et al. 2015). These models include parametric regression and nonparametric approaches, with the primary goal of optimizing prediction accuracy by maximizing explained variability (e.g., R^2), minimizing prediction error (e.g., RMSE), and reducing systematic bias (Zolkos et al. 2013), for specific forest attributes, forest types, and study sites (Næsset et al. 2005, Hudak et al. 2008, Penner et al. 2013, White et al. 2017). In this study, our objective was to investigate the impact of VFS stratification on estimation accuracy and to develop models for simplicity and clarity. Therefore, we focused on parametric models, specifically multivariate multiplicative power models known for their flexibility (Hollaus et al. 2009).

A total of ten LiDAR-derived metrics were utilized in this study, including the mean height of point clouds (*H*mean), the 95th height percentile (*hp*95), the standard deviation (*H*std), and the coefficient of variation (*Hcv*) of point cloud height distribution; the canopy cover (*CC*), the 50th and 75th density percentile (*dp*50 and *dp*75); the mean of the vertical leaf area density (LAD) profile (*LAD*mean) and their standard deviation (*LAD*std) and coefficient of variation (*LAD*cv). They were categorized into three groups of metrics: height, density, and vertical structure-related metrics, each of which accurately depicts the 3D structural aspects of the forest canopy. Through a rule-based exhaustive combination approach as described by Li et al. (2023), a total of 44 formulations of the multiplicative power model, each consisting of 2–5 variables, facilitated the estimations of the VOL, BA, and AGB.

All 44 formulations were fitted using all field plot data from each stratum. The optimal formulation for that stratum was the formulation with the smallest relative root mean square error (rRMSE). The optimal model formulation was log-transformed in order to address the heteroscedasticity in the field plot data, to ensure the normality of the residuals, and to stabilize the variance of the forest attributes. The logarithmic transform was chosen to accommodate the nonlinearity of the response. The model fitting was performed using the maximum likelihood method. However, due to the systematic bias resulting from the log transformation, a correction factor (*CF*) was applied during the back-transformation of the final model by exponentiating both sides of the log-log regression model. The estimate values ($\hat{y}$) were finally multiplied by the following *CF* (Bouvier et al. 2015):

$$CF = \exp\left(\frac{\sum_{i=1}^{n}\left(\ln y_i - \ln \hat{y}_i\right)^2}{(n-p)\times 2}\right) \tag{1}$$

where p is the number of parameters in the final model, and n is the number of field plots. The goodness-of-fir statistics include R^2, rRMSE and mean percentage error (MPE). MPE indicates forecast bias.

$$MPE = \frac{100}{n}\sum_{i=1}^{n}\frac{(y_i - \hat{y}_i)}{y_i} \tag{2}$$

where y_i is the field measurement value of VOL, BA, and AGB, and $\hat{y}_i$ is the predicted value.

To ensure an unbiased assessment of the predictive capability of the model, a specific subset of the field plot dataset was dedicated to model validation. In scenarios where the sample size exceeded 100, 70% of the field plots were randomly selected from the field plot data to serve for model calibration, while the remaining 30% were used for model validation subject to 5 iterations. In cases where the sample size ranged from 50 to 99, the model validation employed a ten-fold cross-validation method. For sample sizes below 50, model validation adopted a leave-one-out cross-validation (LOOV) method. Statistical metrics employed for model validation included R^2, rRMSE, and MPE, whose averaged values were calculated across all iterations.

In this study, Chinese fir, Masson pine, and eucalyptus forests were the single dominant species. Nearly all broad-leaved forests were natural mixed forests, consisting of a diversity of species with a variety of dominant species. However, only an allometric equation was used to calculate their VOL, as was the case for the AGB. Therefore, we refer to the model developed using all field plot data for each forest type as the species-specific model. Correspondingly, the model developed using field plot data from each class and cluster of vertical forest was referred to as the stratum-specific and cluster-specific models, respectively.

Statistical analysis of measurement forest attributes and LiDAR metrics

To analyze the variation in the field-measured attributes and LiDAR metrics after stratification of the vertical forest structure, the coefficient of variation among them was compared and analyzed for all strata.

Pearson's correlation coefficients were used to analyze the statistical relationship between the LiDAR metrics and field-measured attributes for all strata.

Result

Comparative analysis of model accuracy

The rRMSEs of the species-specific model for VOL, BA, and AGB estimations were around 20% for Chinese fir, Masson pine, and eucalyptus forests. In the context of the complex structures exhibited by broad-leaved forests, the rRMSEs of their species-specific VOL, BA, and AGB models were marginally higher, ranging from 28.57% to 35.09% (Table 3 and Supp. Table 1). Notably, the validation statistics, including R^2 and rRMSE, were closely aligned with the goodness-of-fit statistics of those models across all three forest attributes and the four forest types. Although the later metrics slightly outperformed the former (Supp. Table 1), the consensus indicates the robust performance of the species-specific models.

between the stratum- and species-specific models (ΔrRMSE:

$$\Delta rRMSE(\%) = \frac{(rRMSE\,\mathrm{sp} - rRMSE\,\mathrm{st})}{rRMSE\,\mathrm{sp}} \times 100$$

Table 3 Plot level validation rRMSE and MPE of species- and stratum-specific linear regression (log-transformed) models for estimating forest inventory attributes.

Species	Stratum	Sample size	VOL			BA			AGB		
			R^2	rRMSE (%)	MPE (%)	R^2	rRMSE (%)	MPE (%)	R^2	rRMSE (%)	MPE (%)
Chinese fir	ALL	222	0.719	22.84	-1.2	0.545	18.33	-0.7	0.619	20.75	-1.1
	OT_1/M_1	108	0.777	19.36	-4.3	0.483	14.63	-1.9	0.618	17.06	-2.3
	UT_1	61	0.608	23.78	-5.2	0.483	14.63	-1.9	0.685	19.33	-1.3
	OT_1T_2	53	0.466	25.12	-6.9	0.524	22.86	-6.1	0.411	21.93	-5.7
	M_2	114	0.706	24.89	-4.3	0.558	21.59	-2.4	0.690	22.17	-2.6
Masson pine	ALL	260	0.845	19.03	-3.6	0.705	17.38	-3.4	0.694	20.67	-4.7
	OT_1/M_1	149	0.757	17.85	-4.6	0.523	16.46	-5.0	0.452	18.78	-6.0
	UT_1	36	0.759	20.39	-5.1	0.743	15.37	-4.1	0.667	21.46	-4.9
	OT_1T_2	37	0.759	16.67	-5.1	0.511	15.52	-5.5	0.544	16.59	-5.6
	$T_1T_2T_3$	38	0.837	15.92	-4.8	0.706	13.44	-3.2	0.615	19.68	-6.0
	M_2	111	0.884	18.75	-4.0	0.840	13.86	-1.1	0.791	18.80	-2.2
Eucalyptus	ALL	269	0.837	17.97	-3.1	0.755	16.86	-2.7	0.725	23.32	-5.8
	OT_1/M_1	212	0.794	17.63	-3.3	0.706	16.74	-2.5	0.671	23.17	-7.7
	OT_1T_2	30	0.779	21.17	-5.1	0.757	19.75	-2.3	0.811	20.66	-1.5
	T_1T_3	27	0.748	16.60	-3.1	0.386	20.66	-8.4	0.418	25.77	-14.5
	M_2	57	0.887	17.22	-2.8	0.843	15.88	-2.6	0.841	20.26	-4.5
Broad-leaved	ALL	252	0.527	35.09	-11.0	0.445	28.57	-8.1	0.414	33.49	-10.7
	OT_1/M_1	42	0.636	26.23	-7.0	0.632	19.90	-5.9	0.687	22.98	-9.7
	UT_1	43	0.692	29.97	-16.1	0.685	24.38	-8.7	0.685	25.51	-7.4
	OT_1T_2/M_2	80	0.402	37.12	-18.1	0.398	30.65	-3.1	0.367	37.33	-17.9
	UT_1T_2	40	0.422	37.21	-22.4	0.223	34.32	-21.1	0.178	39.09	-25.9
	$T_1T_2T_3$	47	0.410	28.66	-6.2	0.364	23.83	-3.5	0.354	28.32	-6.8
	M_3	130	0.588	35.94	-16.8	0.401	30.17	-14.7	0.448	34.29	-17.1

The performance of the stratum-specific models for most VFS classes is also robust. Although the rRMSEs of some models were larger than those of the species-specific models, the rRMSEs of the stratum-specific models for the three forest attributes estimations in Chinese fir, Masson pine, and eucalyptus forests were approximately 20%. In broad-leaved forests, the rRMSEs of most stratum-specific models were less than 35%. Furthermore, the validation statistics, R^2 and rRMSE, were close to the goodness-of-fit statistics (Table 3, Fig. 4, and Supp. Table 1).

After calculating the difference in rRMSE where *rRMSE* sp was the rRMSE of the species-specific model and *rRMSE* st was the rRMSE of the stratum-specific model), we found that 64% of stratum-specific models showed a decrease in rRMSE compared to species-specific models, reductions ranged from 0.7% to31.4%. 36% of the stratum-specific models had a larger RMSE than the tree-specific models, with an increase ranging from 2.4% to 24.7%. (Table 4). Generally, the performances of stratum-specific models for Masson pine and broad-leaved forests were better than that for Chinese fir and eucalyptus forests. Among the 12 stratum-specific models

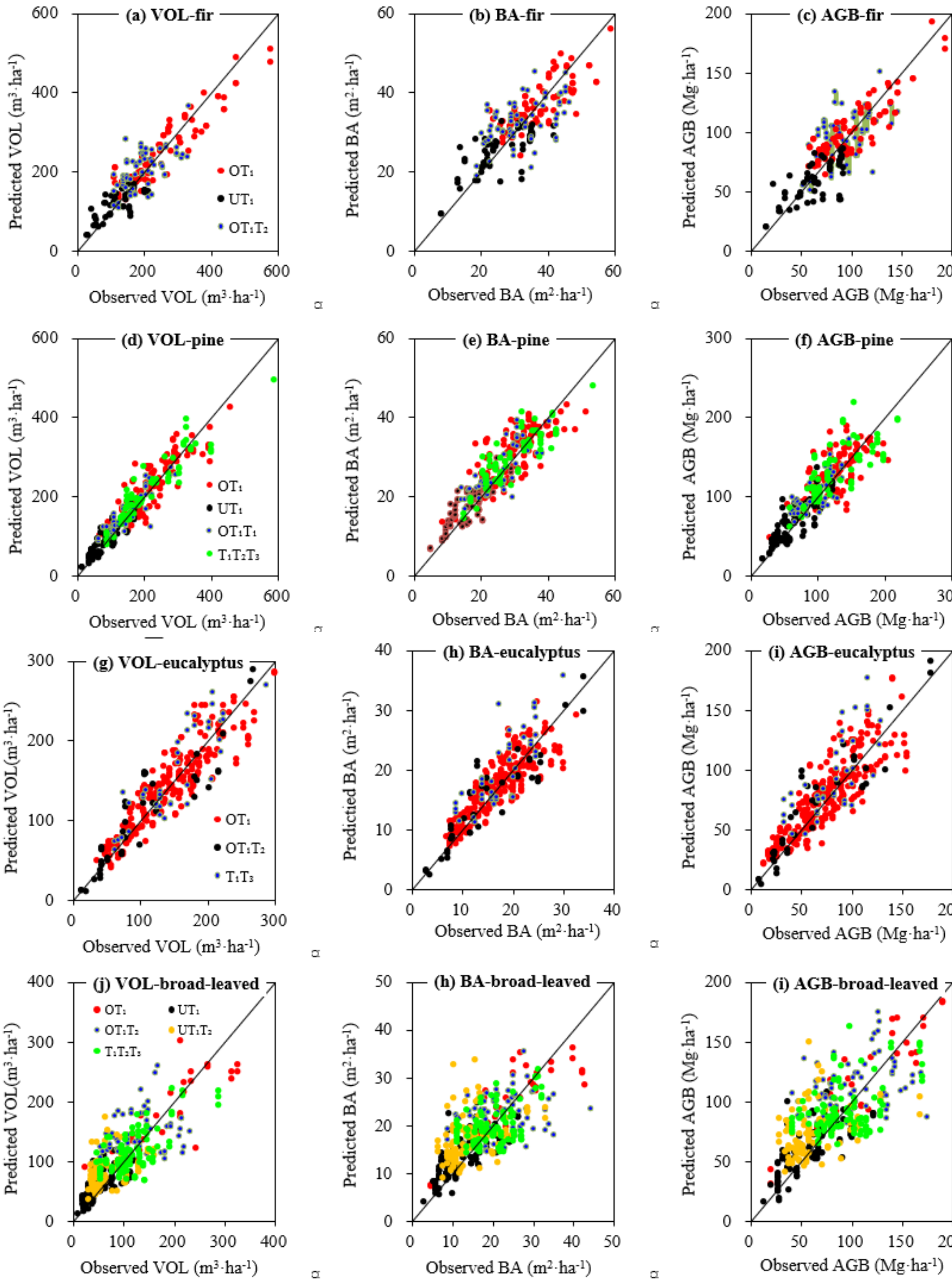

Figure 4 Observed vs. predicted stand volume (VOL), basal area (BA) and aboveground biomass (AGB) for field plots with Chinese fir, Masson pine, eucalyptus, and broad-leaved as main species or species group. Predictions were the log-transformed inverse value based on the validation dataset.

for pine forests, ten models had an rRMSE smaller than that of the species-specific model, while among the 15 stratum-specific models for broadleaf forests, nine models had an rRMSE smaller than that of the species-specific model. In contrast, only five of the nine models in the Chinese fir and eucalyptus forests had an rRMSE smaller than those of the species-specific model, respectively. The above results demonstrated that vertical forest structure stratification helps to improve the accuracy of forest attribute estimations. Overall, strata with lower estimation accuracies than the species-specific models were mostly strata with a smaller number of field plots.

Table 4 Relative difference of rRMSE between the species-specific models and stratum-specific models.

Species	Stratum	ΔrRMSE (%)		
		VOL model	BA model	AGB model
Chinese fir	OT_1/M_1	-15.2	-20.2	-17.8
	UT_1	4.1	-20.2	-6.8
	OT_1T_2	10.0	24.7	5.7
	M_2	9.0	17.8	6.9
Masson pine	OT_1/M_1	-6.2	-5.3	-9.2
	UT_1	7.1	-11.6	3.8
	OT_1T_2	-12.4	-10.7	-19.8
	$T_1T_2T_3$	-16.4	-22.7	-4.8
	M_2	-1.5	-20.3	-9.0
Eucalyptus	OT_1/M_1	-1.9	-0.7	-0.7
	OT_1T_2	17.8	17.1	-11.4
	T_1T_3	-7.6	22.6	10.5
	M_2	-4.2	-5.8	-13.1
Broad-leaved	OT_1/M_1	-25.2	-30.3	-31.4
	UT_1	-14.6	-14.7	-23.8
	OT_1T_2/M_2	5.8	7.3	11.5
	UT_1T_2	6.1	20.1	16.7
	$T_1T_2T_3$	-18.3	-16.6	-15.4
	M_3	2.4	5.6	2.4

In most strata, the performances of the stratum-specific models in estimating three forest attributes (VOL, BA, and AGB) were consistent. When the rRMSE of the stratum-specific model for one attribute estimation was lower than that of the species-specific model, the rRMSE of the stratum-specific model for the remaining two attribute estimations was also lower than that of the species-specific model. Similarly, if the rRMSE of the stratum-specific model for one attribute estimation was higher than that of the species-specific model, the rRMSEs of the stratum-specific model for the remaining two attribute estimations were also higher than that of the species-specific model. However, there were exceptions to this trend, such as in the UT_1 stratum of Chinese fir and Masson pine forests, as well as the OT_1T_2 and T_1T_3 strata of eucalyptus forests. In these cases, the rRMSEs of the stratum-specific models for one or two attribute estimations may be lower than those of the species-specific model, while the rRMSE of the remaining attribute estimation was larger than that of the species-specific model.

After clustering multiple vertical forest structure classes into a new class (cluster), the rRMSEs of the cluster-specific model for three forest attribute estimations for the new class (M_2) in Masson pine and eucalyptus forests were lower than those of the species-specific models. However, the performances of the models for the new class of Chinese fir forests (M_2) and broad-leaved forests (M_3) were the opposite (Table 4).

Based on the number of field plots of all classes and clusters of vertical forest structure, we calculated the weighted average rRMSE for three attribute estimations of four forest types (species). After comparing the weighted average rRMSE and the rRMSE of the species-specific model, we found that in ten out of 12 attribute estimations for the four forest types, the weighted average rRMSEs were smaller than those of the species-specific model, with a maximum reduction of 9.4%. This suggested that the stratification-based estimation method, which was founded on vertical forest structure, could improve the accuracy of forest attribute estimation. When we clustered the vertical forest structures, we found that in 11 out of the 12 forest attributes, the weighted average rRMSEs were lower than those of the species-specific model, with a maximum reduction of 11.7%. Although overall their weighted average rRMSEs were reduced to a lesser extent than those of the stratum-specific model (Table 5), this still demonstrated that clustering the vertical forest structure into two or three classes could improve the accuracy of estimating forest attributes to some extent.

Both Chinese fir and eucalyptus forests are planted and have only three vertical structure types, as shown in Table 2 and Fig. 3. They have relatively simple vertical forest structure. After VFS stratification, the weighted average rRMSEs for the VOL, BA and AGB estimation were reduced by 3.7%, -0.7% and 8.7% for fir forests compared with those of the species-specific model, respectively. Similarly, for eucalyptus forests, their rRMSEs were reduced by 0.3%, -3.6% and 0.7%, respectively. Most of Masson pine and broad-leaved forests are natural forests that have a more complex vertical structures as compared to planted forests, with four and five vertical structure classes, respectively. After stratification of vertical forest structure was implemented, the weighted average rRMSEs of VOL, BA and AGB estimations were reduced by 6.6%, 9.4% and 8.1% for pine forests and 7.3%, 5.1% and 5.9% for broad-leaved forests compared to those of the species-specific model, respectively (Table 5).

The MPEs for most of the stratum-specific models were larger than those for the species-specific models, although there were some exceptions.

In summarizing the performance of the stratum-and cluster-specific models, several key points emerge:

(1) More than 60% of stratum-specific models had rRMSEs that were lower than those of the species-specific models across all four forest types (species), regardless of whether VOL, BA, or AGB estimations. In addition, the weighted average rRMSEs based on the number of plots for all strata were less than those of the species-specific models. It was found that most of the stratum-specific models with rRMSEs larger than those of the species-specific models were in strata with a small number of field plots.

(2) Except the BA of broad-leaved forests, the weighted average rRMSEs for all three forest attribute estimations across all four forest types consistently showed lower values than those of the species-specific models after clustering the vertical forest structures into two or three clusters.

(3) The level of complexity in vertical forest structures had a direct impact on the rRMSE reduction achieved through stratification. Forest types with complex vertical structures, such as broad-leaved and Masson pine forests, experienced substantial weighted average rRMSE reductions when using stratum-specific modes. Conversely, forest types with relatively

Table 5 Weighted average rRMSE of VFS classes and clusters vs. rRMSE of species-specific mode for three forest attribute estimations.

Forest type	Attribute	rRMSE of species-specific model (all) (%)	Weighted average rRMSE of Stratum-specific model(%)	ΔrRMSE (%)	Weighted average rRMSE of cluster-specific model (%)	ΔrRMSE (%)
Chinese fir	VOL	22.84	22.00	-3.7	22.2	-2.8
	BA	18.33	18.45	0.7	18.2	-0.7
	AGB	20.75	18.94	-8.7	19.7	-5.1
Masson pine	VOL	19.03	17.78	-6.6	18.2	-4.2
	BA	17.38	15.74	-9.4	15.4	-11.7
	AGB	20.67	19.00	-8.1	18.8	-9.1
Eucalyptus	VOL	17.97	17.92	-0.3	17.5	-2.4
	BA	16.86	17.47	3.6	16.6	-1.8
	AGB	23.32	23.15	-0.7	22.6	-3.3
Broad-leaved	VOL	35.09	32.52	-7.3	34.7	-1.1
	BA	28.57	27.10	-5.1	28.6	0.2
	AGB	33.49	31.52	-5.9	33.4	-0.3

simple vertical structures, like eucalyptus and Chinese fir forests, exhibited a lower weighted average rRMSE reduction with stratum-specific models.

Variation in forest attributes and LiDAR metrics

In most strata, excluding the UT_1 stratum in the Chinese fir, Masson pine, and broad-leaved forests, as well as the OT_1T_2 stratum in the eucalyptus forests, the coefficients of variation for all three field-measured attributes (VOL, BA, and AGB) were smaller compared to those of the non-stratification case. This observation implied that the introduction of VFS stratification generally led to a reduction in the variability of the field-measured attributes across most of the strata. The extent of attribute variation across different VFS classes was shown to depend on the forest type. Notably, the least variation was evident in the OT_1 stratum within the fir and pine forests, while in eucalyptus and broad-leaved forests, the T_1T_3 and $T_1T_2T_3$ strata exhibited the least variability, respectively (Table 6).

Similar to the variability of field-measured attributes, most LiDAR metrics exhibited reduced variability in most strata, except for the UT_1 stratum in fir, pine, and broad-leaved forests, as well as the OT_1T_2 stratum in eucalyptus forests, when compared to the non-stratified case. Notably, in all but the OT_1T_2 stratum in the eucalyptus forest, both *H*mean and *hp*95 showed smaller variations compared to the non-stratification case, while *H*std and *Hcv* exhibited larger variations in most strata than in the case without stratification. In all forest types except broad-leaved forests, the newly formed stratum (M_3) resulting from the cluster analysis exhibited greater variations in all three field-measured attributes and the majority of LiDAR metrics compared to the variation in field-measured attributes and LiDAR metrics without stratification (Table 6).

The observed variations in field-measured attributes and LiDAR metrics collectively suggest a reduction in the heterogeneity

Table 6 Comparison of coefficient of variation and mean of field-measured attributes and LiDAR metrics for all classes of vertical forest structure.

Forest type	Stratum	Coefficient of variation									Mean			
		VOL	BA	AGB	*H*mean	*hp*95	*CC*	*dp*50	*dp*75	*LAD* mean	*H*std	*H*cv	*LAD*std	*LAD*cv
Chinese fir	All	46.58	29.33	35.35	31.76	28.86	7.29	33.33	71.43	43.28	2.18	0.24	0.64	0.95
	OT_1/M_1	39.76	21.05	27.55	27.75	26.17	7.22	21.33	63.16	42.67	1.99	0.19	0.76	1.01
	OT_1T_2	32.35	24.29	27.81	17.74	19.07	3.06	21.31	50.00	32.76	2.80	0.28	0.52	0.86
	UT_1	45.00	35.67	39.69	26.87	26.97	12.09	50.00	83.33	41.94	1.85	0.30	0.56	0.93
	M_2	46.70	32.82	40.19	31.72	30.71	8.42	37.25	60.00	38.33	2.36	0.29	0.53	0.89
Masson pine	All	46.94	31.70	35.70	30.13	26.95	9.68	28.13	57.69	50.00	3.04	0.27	0.41	0.89
	OT_1/M_1	37.50	26.10	28.81	23.81	22.40	10.75	19.18	43.75	56.25	2.75	0.22	0.46	0.96
	OT_1T_2	36.96	28.32	27.86	23.42	24.22	5.26	26.32	52.94	43.48	3.31	0.30	0.39	0.81
	$T_1T_2T_3$	45.21	27.85	34.84	24.73	20.10	7.53	24.14	50.00	41.18	4.73	0.38	0.28	0.81
	UT_1	43.23	31.79	38.50	21.38	20.83	12.64	33.33	70.00	34.78	2.28	0.33	0.34	0.73
	M_2	56.82	36.26	43.36	34.85	32.28	9.78	30.77	66.67	40.48	3.43	0.34	0.33	0.78
Eucalyptus	All	44.15	34.11	45.47	24.52	22.46	10.84	21.15	44.12	34.78	3.48	0.25	0.26	1.15
	OT_1/M_1	41.97	31.93	43.17	22.67	21.00	10.84	18.52	41.67	34.78	3.12	0.21	0.28	1.24
	OT_1T_2	64.97	52.93	69.45	36.86	34.35	15.85	28.26	54.17	32.00	3.84	0.31	0.20	0.82
	T_1T_3	38.63	28.93	37.05	20.93	16.78	7.95	15.56	40.00	29.17	5.94	0.44	0.21	0.87
	M_2	52.43	41.97	53.99	29.78	27.20	12.94	21.74	48.15	33.33	4.83	0.37	0.20	0.84
Broad-leaved	All	58.91	41.13	48.26	35.84	30.81	14.29	41.18	93.33	40.00	3.05	0.31	0.39	0.84
	OT_1/M_1	45.58	32.10	38.84	24.38	20.91	14.89	25.68	70.97	40.00	3.20	0.23	0.47	0.92
	UT_1	57.79	48.63	50.98	18.02	24.34	27.27	65.52	83.33	55.26	1.97	0.34	0.32	0.88
	OT_1T_2/M_2	42.03	33.39	40.29	21.79	22.41	4.17	21.31	61.11	33.33	3.14	0.28	0.44	0.82
	UT_1T_2	45.67	39.61	45.74	15.05	12.63	8.89	30.77	75.00	36.36	2.61	0.36	0.37	0.81
	$T_1T_2T_3$	43.81	29.32	34.79	17.71	17.14	7.45	27.91	63.64	33.33	4.12	0.38	0.30	0.81
	M_3	59.08	41.76	47.70	29.59	30.31	8.35	26.68	61.76	59.63	3.16	0.25	0.42	0.96

of forest structures following the VFS classification across the majority of strata.

Statistical relationships between forest attributes and LiDAR metrics

The Pearson correlation coefficients between the field-measured attributes and most LiDAR metrics in most strata showed a generally stronger connection when stratified than when not. Eucalyptus forests, among the four forest types, exhibited the simplest VFS. In the OT_1T_2 and T_1T_3 strata of the eucalyptus forests, the correlation coefficients between the three field-measured attributes and ten LiDAR metrics, excluding *hp*95 and *Hmean*, were generally higher compared to the non-stratification scenario. In the OT_1 stratum, while the correlation coefficients between the field-measured attributes and most LiDAR metrics were somewhat reduced compared to the non-stratified case, there were notable improvements for metrics like *Hmean*, *LADmean*, and *LADcv*. Upon clustering the OT_1T_1 and T_1T_3 strata into a new single stratum, the correlation coefficients between the ten LiDAR metrics and three field-measured attributes were consistently higher than those in the absence of stratification (Table 7).

Table 7 Comparison of Pearson correlation coefficients between field-measured attributes and LiDAR metrics for vertical forest structure classes in eucalyptus and broad-leaved forests.

Forest type	Attrib.	Stratum	*hp*95	*H*mean	*H*std	*H*cv	*dp*50	*dp*75	*CC*	*LAD*mean	*LAD*std	*LAD*cv
Eucalyptus	VOL	ALL	0.849	0.871	0.517	0.037	0.423	0.672	0.597	-0.064	0.323	0.451
		OT_1/M_1	0.845	0.887	0.511	0.031	0.377	0.649	0.583	-0.113	0.261	0.461
		OT_1T_2	0.903	0.909	0.849	0.074	0.663	0.830	0.718	0.107	0.564	0.535
		T_1T_3	0.820	0.768	0.861	0.151	0.518	0.768	0.485	0.159	0.503	0.578
		M_2	0.880	0.860	0.820	0.250	0.590	0.818	0.671	0.116	0.526	0.551
	BA	ALL	0.782	0.804	0.469	0.024	0.456	0.675	0.632	0.018	0.387	0.430
		OT_1/M_1	0.753	0.805	0.439	0.003	0.414	0.667	0.609	-0.035	0.347	0.454
		OT_1T_2	0.895	0.886	0.844	0.083	0.678	0.811	0.742	0.163	0.560	0.482
		T_1T_3	0.739	0.683	0.764	0.135	0.560	0.714	0.585	0.308	0.533	0.479
		M_2	0.862	0.833	0.777	0.226	0.625	0.784	0.719	0.200	0.531	0.482
	AGB	ALL	0.816	0.825	0.514	0.063	0.430	0.655	0.571	-0.071	0.298	0.407
		OT_1/M_1	0.804	0.839	0.499	0.052	0.400	0.638	0.547	-0.133	0.237	0.422
		OT_1T_2	0.885	0.879	0.845	0.112	0.624	0.810	0.681	0.124	0.560	0.508
		T_1T_3	0.755	0.719	0.785	0.115	0.571	0.766	0.485	0.208	0.498	0.531
		M_2	0.857	0.835	0.789	0.240	0.586	0.802	0.652	0.143	0.519	0.516
Broad-leaved	VOL	ALL	0.718	0.633	0.108	-0.007	0.030	0.019	0.012	0.009	0.011	0.005
		OT_1/M_1	0.774	0.814	0.437	-0.469	0.535	0.634	0.306	0.173	0.349	0.452
		UT_1	0.281	0.674	0.176	-0.265	0.623	0.596	0.523	0.451	0.195	-0.289
		OT_1T_2/M_2	0.426	0.475	0.337	-0.090	0.273	0.178	0.263	0.028	0.087	0.080
		UT_1T_2	0.311	0.371	0.056	-0.009	0.040	0.015	0.015	0.017	-0.016	-0.041
		$T_1T_2T_3$	0.622	0.722	0.589	0.013	0.414	0.522	0.181	0.060	0.049	0.006
		M_3	0.645	0.496	0.136	-0.004	0.025	0.011	0.014	0.008	0.006	-0.004
	BA	ALL	0.610	0.536	0.090	-0.007	0.029	0.015	0.014	0.013	0.015	0.005
		OT_1/M_1	0.652	0.691	0.316	-0.484	0.611	0.498	0.468	0.376	0.501	0.474
		UT_1	0.270	0.630	0.147	-0.273	0.633	0.617	0.571	0.518	0.282	-0.256
		OT_1T_2/M_2	0.363	0.381	0.271	-0.092	0.193	0.071	0.342	0.126	0.194	0.183
		UT_1T_2	0.225	0.289	0.031	-0.009	0.035	0.013	0.017	0.025	-0.003	-0.030
		$T_1T_2T_3$	0.463	0.584	0.418	-0.066	0.424	0.452	0.254	0.211	0.206	0.126
		M_3	0.541	0.427	0.105	-0.004	0.024	0.009	0.015	0.013	0.011	-0.001
	AGB	ALL	0.638	0.550	0.100	-0.006	0.028	0.016	0.012	0.010	0.012	0.004
		OT_1/M_1	0.711	0.747	0.374	-0.465	0.580	0.560	0.386	0.303	0.451	0.466
		UT_1	0.370	0.674	0.262	-0.161	0.576	0.581	0.537	0.419	0.190	-0.230
		OT_1T_2/M_2	0.349	0.365	0.285	-0.048	0.197	0.079	0.247	0.051	0.111	0.095
		UT_1T_2	0.244	0.268	0.052	-0.005	0.030	0.014	0.010	0.012	-0.015	-0.034
		$T_1T_2T_3$	0.558	0.622	0.547	0.090	0.326	0.476	0.161	0.079	0.104	0.079
		M_3	0.561	0.425	0.118	-0.003	0.022	0.009	0.013	0.009	0.007	-0.003

Broad-leaved forests exhibited the most complex VFS. In contrast to the Pearson correlation coefficients between the field-measured attributes and the LiDAR metrics in the absence of stratification in the broad-leaved forest, all correlation coefficients increased in the OT_1 stratum. In the OT_1T_2, $T_1T_2T_3$, and UT_1 strata, all correlation coefficients exhibited an increase beyond *hp*95. While some correlation coefficients increased in the UT_1T_2 stratum. Upon clustering the OT_1T_2, $T_1T_2T_3$, UT_1, and UT_1T_2 strata into a new stratum (M_2), a majority of the correlation coefficients decreased, except for *H*std and *CC* (Table 6). The changes in the Pearson correlation coefficients between the field-measured attributes and the LiDAR metrics after VFS stratification in the Chinese fir and Masson pine forests were similar to those observed in the eucalyptus and broad-leaved forests. This suggested that the statistical relationship between the field-measured attributes and the LiDAR metrics becomes stronger after stratification.

Discussion

Numerous previous studies have consistently highlighted that stratification based on forest type and dominant species can enhance the accuracy of airborne LiDAR forest attribute estimation (Jiang et al. 2020, Chen et al. 2022). Furthermore, some studies have underscored that stratification based on dominant species and maturity class can yield even greater improvements in accuracy (Hauglin et al. 2021). Our study not only corroborated these findings but also demonstrated that the accuracy of forest attribute estimation experienced notable enhancements through tree species-based vertical forest structure stratification.

Performances of the species-specific models

Over the past decade, numerous studies have emerged focusing on airborne LiDAR-based forest attribute estimation in subtropical regions, although often within a limited spatial extent. For instance, in studies conducted across planted forests in Guangxi (5000 ha in area) and Jiangsu Province (1260 ha) in China, the rRMSEs for VOL estimations using multiple linear regression models were 21.34% and 16.47%, respectively (Liu et al. 2021, Zhang et al. 2017). Similarly, the rRMSEs for aboveground biomass estimations in Chinese fir, Masson pine, and eucalyptus forests were 15.86%, 21.7%, and 25.66%, respectively (Jing et al. 2022). However, although the estimation accuracies of these studies were close to those of the present study, they exhibited limited comparability with our present study due to their restricted study area and notable forest homogeneity.

In contrast, studies encompassing temperate forests with study areas exceeding 5,000 km^2 showed varied levels of accuracy in estimating forest attributes using parametric models. The rRMSEs for VOL and BA estimations ranged from 11.04%–46.7% and 13.8%–37.1%, respectively, across these diverse investigations (Woods et al. 2008, Dalponte et al. 2011, Nord-Larsen & Schumacher, 2012, Treitz et al. 2012, Watt & Watt, 2013, Nilsson et al. 2017, Hill et al. 2018, Hauglin et al. 2021). Zolkos et al. (2013) synthesized findings from 34 studies worldwide on discrete airborne LiDAR-based AGB estimations, revealing a mean residual standard error (RSE) of 27%. This wide variation in model accuracy is attributed to a variety of factors, such as forest type, species, stand structure and characteristics, site, and more.

In the context of our study, which focused on Chinese fir, Masson pine, eucalyptus, and broad-leaved forests, the rRMSEs of the species-specific models used for VOL estimation were 22.84%, 19.03%, 17.97%, and 35.09%, respectively. For the BA estimations, they were 18.33%, 17.38%, 16.85%, and 28.57%, respectively. For the AGB estimation, they were 20.75%, 20.67%, 23.32%, and 33.49%, respectively (Table 3). We are confident that the accuracy achieved by all species-specific models in this study is indeed noteworthy when considering the wide range of published studies and taking into account the substantial extent of our study area along with the inherent heterogeneity in forest structure.

Accuracy improvement for VFS stratification-based estimation of forest attributes

Forest attributes are closely related to a variety of factors, such as species composition, stand structure and characteristics, study sites, and more. Therefore, stratification of field plots according to forest types and dominant tree species can reduce the heterogeneity of stand characteristics within the stratum and improve the accuracy of forest attribute estimation (Chen et al. 2022, Jiang et al. 2020), which has become a consensus in the application of airborne LiDAR-based forest attribute estimations. Hauglin et al. (2021) demonstrated that by stratifying forest stands based on main species and maturity classes (such as young and mature forests), the rRMSEs of stratum-specific models for estimating VOL, Lorey's height, BA, and AGB were reduced by up to 1.6 percentage points (pp) (equal to 4.0%), 0.5 pp (4.4%), 0.5 pp (1.5%), and 1.8 pp (4.6%), when compared to the species-specific models. Our findings, in turn, suggested that stratified forest stands based on vertical canopy structure reduced the weighted average rRMSEs of the stratum-specific models for VOL, BA, and AGB estimations by 0.3%-7.3%, +3.6%-9.4% (Chinese fir and eucalyptus forest had increased 0.7% and 3.6%), and 0.7%-8.7%, respectively, when compared to the rRMSEs of the corresponding species-specific models. Notably, our stratum-specific models exhibited slightly superior performance compared to those of Hauglin et al. (2021), indicating that stratification based on vertical forest structure surpasses age-based stratification.

Subsequent stratification of the vertical canopy structure within stands showed a decrease in the coefficient of variation of forest attributes across all forest types in most strata compared to the case without stratification. This decline was also observed for key LiDAR-derived height-related metrics (*H*mean and *hp*95) in nearly all strata, alongside density-related metrics (*CC*, *dp*50, and *dp*75) and the mean leaf area density (*LAD*mean) in most strata (Table 6). These variations in field-measured attributes and LiDAR metrics imply that stratification has the capacity to mitigate the three-dimensional structural diversity within a given stratum. The Pearson correlation coefficients between forest attributes and LiDAR metrics (excluding *hp*95) from field plots were significantly higher in most strata compared to cases without stratification, which can be attributed to the reduction in heterogeneity after stratification (Table 7). This suggested that vertical structure stratification significantly enhances the statistical relationship between forest attributes and LiDAR metrics, serving as a principal catalyst for the enhancement in the accuracy of forest attribute estimations.

Similar to the studies of Hauglin et al. (2021) and Nord-Larsen and Schumacher (2012), this study also observed instances where the accuracy of the stratum-specific models for forest attribute estimation was marginally lower than that of the species-specific models for some strata (Tables 3 and Supp Table 1). This could potentially be attributed to the fact that coefficients of variation of the forest attributes and LiDAR metrics in some strata did not exhibit a decrease post-stratification (Table 6), and not all their statistical relationships experienced an enhancement (Table 7). These instances could be attributed to two primary factors: firstly, the substantial heterogeneity of the forest structures within certain strata owing to the limited number of field plots in some strata, necessitating the amalgamation of similar strata, as seen in the OT_1T_2 stratum of eucalyptus forests, which essentially encompasses three strata, OT_1T_2, UT_1, and UT_1T_2; and secondly, the small sample size in some strata also significantly affects the accuracy of the forest attribute estimation.

It is important to note that this study specifically addresses the multiplicative power models that rely on the statistical relationships between forest attributes and LiDAR variables. The effect of VFS stratification on the accuracy of forest attribute estimations for machine learning models that rely on weaker statistical relationships remains an avenue to be investigated.

Applications of VFS stratification-based estimation

There are two strategies to implement the proposed framework for stratification-based estimation of forest attributes in airborne LiDAR-based large-scale forest resource inventory and monitoring:

(1) If the timeframe for collecting airborne LiDAR and field plot data is not too long, if forest alterations are gradual (e.g., infrequent timber harvesting and forest regeneration), or if forest tree growth is moderate (as seen in temperate forests), the approach outlined by Zhou and Li (2023) can be employed to generate the wall-to-wall map of the vertical forest structures across the entire study areas using LiDAR data. Subsequently, field plots are allocated based on this stratification, taking potential additional factors like *Hmean*, *CC*, etc., into consideration. These field plots are then measured to acquire the required data. Finally, specific models for each stratum are developed to estimate the forest attributes.

(2) If field campaigns and airborne LiDAR data acquisition occur concurrently, similar to the methodology employed in this study, a post-stratification procedure is employed for the stratification-based forest attribute estimations. This approach is suitable when the sample size is sufficiently large, generally exceeding 50 plots per stratum and enabling coverage of at least two strata. The procedure unfolds in two stages: Firstly, the classification method detailed by Zhou and Li (2023) is utilized to classify the vertical forest structures of the field plot. The outcomes of this classification are then fine-tuned through the visual interpretation method. Secondly, specific models are developed for each stratum to estimate forest attributes.

Conclusion

This study effectively demonstrated the utility of VFS stratification in enhancing the accuracy of forest attribute estimation using airborne LiDAR data across various forest types, including three key attributes: stand volume, basal area, and above-ground biomass. Through the application of VFS classification, it was evident that the weighted average accuracies achieved via the stratum-based estimation of the three forest attributes of four forest types were higher than those achieved using species-based estimation methods. Although it was acknowledged that certain strata might had lower estimation accuracy than species-based methods due to the limited sample size, the overall trend remained one of improvement. Even after clustering VFSs into two or three classes using cluster analysis for all forest types, the resulting accuracy, although reduced compared to pre-clustering, still exceeded that of species-based estimation.

The primary factors driving the increased accuracy of the post-stratification were the reduction of heterogeneity within the strata stand structure and the strengthening of the statistical relationship between field-measured attributes and LiDAR-derived metrics.

By presenting these findings, this study represents a significant advancement in improving the accuracy of forest inventory attribute estimation in a large region utilizing airborne LiDAR data. However, it is important to note that the conclusions of this study are restricted to the multivariate power models and should be further validated using machine learning models. This highlights the potential for further refinements and extensions of the framework.

Acknowledgment

This project is a part of the project "the Fifth Forest Management Inventory of Guangxi Zhuang Autonomous Region, China (5th FMI-GX 2017-2020)". The airborne LiDAR data that were acquired and preprocessed and the field data measurements were funded by the Department of Finance of Guangxi Zhuang Autonomous Region, China. The authors would like to express their sincere gratitude to Chengling Yang and Yao Liang from the Guangxi Forest Inventory and Planning Institute (FIPI-GX) and to the 120 field crews who worked on the field measurements. The authors also thank Guangxi 3D Remote Sensing Engineering Technology Co., Ltd.; Feiyan Aero Remote Sensing Technology Co., Ltd.; Zhongke Remote Sensing Technology Group Co., Ltd.; and Guangzhou Jiantong Surveying and Mapping Geographic Information Technology Co., Ltd. These companies were responsible for acquiring and preprocessing the airborne LiDAR data utilized herein. We thank the anonymous reviewers and editors for their insightful suggestions.

Declaration of the authors

The authors declare there is no conflict of interest regarding the publishing of the paper, which does not include any form of plagiarism.

References

Adnan S., Maltamo M., Mehtätalo L., Ammaturo R.N.L., Packalen P., & Valbuena R. 2021. Determining maximum entropy in 3D remote sensing height distributions and using it to improve aboveground biomass modelling via stratification. Remote Sens. Environ. 260, 112464. https://doi.org/10.1016/j.rse.2021.112464.

Asner G.P., Mascaro J., Muller-Landau H.C., Vieilledent G., Vaudry R., Rasamoelina M., Hall J.S., & van Breugel, M. 2012. A universal airborne LiDAR approach for tropical forest carbon mapping. Oecologia, 168, 1147–1160. https://doi.org/10.1007/s00442-011-2165-z.

Bohlin J., Bohlin I., Jonzén J., & Nilsson M. 2017. Mapping forest attributes using data from stereophotogrammetry of aerial images and field data from the national forest inventory. Silva Fenn. 51(2), 2021. https://doi.org/10.14214/sf.2021.

Bouvier M., Durrieu S., Fournier R.A., & Renaud J-P. 2015. Generalizing predictive models of forest inventory attributes using an area-based approach with airborne LiDAR data. Remote Sens. Environ. 156, 322–334. https://doi.org/10.1016/j.rse.2014.10.004.

Cai H., Mo Z., Nong S., & Zhang W. 2018. Research on forest carbon in Guangxi. Guangxi Science & Technology Publishing House Co., Ltd. Nanning 530023, China, pp. 26-48. (in Chinese).

Chen M., Qiu X., Zeng W., & Peng D. 2022. Combining sample plot stratification and machine learning algorithms to improve forest aboveground carbon density estimation in northeast China using airborne LiDAR Data. Remote Sens. 14, 1477. https://doi.org/10.3390/rs14061477.

Chen Q., Laurin G.V., Battles J.J., & Saah D. 2012. Integration of airborne lidar and vegetation types derived from aerial photography for mapping aboveground live biomass. Remote Sens. Environ. 121, 108–117. https://doi.org/10.1016/j.rse.2012.01.021.

Chirici G., McRoberts R.E., Fattorini L., Mura M., & Marchetti, M. 2016. Comparing echo-based and canopy height model-based metrics for enhancing estimation of forest aboveground biomass in a model-assisted framework. Remote Sens. Environ. 174, 1-9. https://doi.org/10.1016/j.rse.2015.11.010.

Dalponte M., Martinez C., Rodeghiero M., & Gianelle D. 2011. The role of ground reference data collection in the prediction of stem volume with LiDAR data in mountain areas. ISPRS J. Photogramm. 66, 787–797. https://doi.org/10.1016/j.isprsjprs.2011.09.003.

de Lera Garrido, A., Gobakken, T., Ørka, H. O., Næsset, E., Bollandsås, O. M. (2020). Reuse of field data in ALS-assisted forest inventory. Silva Fenn. 54(5), 10272. https://doi.org/10.14214/sf.10272.

Fassnacht F.E., Hartig F., Latifi H., Berger C., Hernández J., Corvalán P., & Koch B. 2014. Importance of sample size, data type and prediction method for remote sensing-based estimations of aboveground forest biomass. Remote Sens. Environ. 154, 102–114. https://doi.org/10.1016/j.rse.2014.07.028.

Fekety P.A., Falkowski M.J., & Hudak A.T. 2015. Temporal transferability of LiDAR-based imputation of forest inventory attributes. Can. J. For. Res. 45, 422–435. https://doi.org/10.1139/cjfr-2014-0405.

Gobakken T., Korhonen L., & Næsset E. 2013. Laser-assisted selection of field plots for an area-based forest inventory. Silva Fenn. 47(5), 943. https://doi.org/10.14214/sf.943.

Gobakken T., & Næsset E. 2008. Assessing effects of laser point density, ground sampling intensity, and field sample plot size on biophysical stand properties derived from airborne laser scanner data. Can. J. For. Res. 38, 1095–1109. https://doi.org/10.1139/X07-219.

Gobakken T., Næsset E., Nelson R., Bollandsås O.M., Gregoire T.G., Ståhl G., Holm S., Ørka H.O., & Astrup R. 2012. Estimating biomass in Hedmark county, Norway using national forest inventory field plots and airborne laser scanning. Remote Sens. Environ. 123, 443–456. https://doi.org/10.1016/j.rse.2012.01.025.

Gökkaya K., Thomas V., Noland T.L., McCaughey H., Morrison I., & Treitz P. 2015. Prediction of macronutrients at the canopy level using spaceborne imaging spectroscopy and LiDAR data in a Mixedwood boreal forest. Remote Sens. 7, 9045-9069. https://doi.org/10.3390/rs70709045.

González-Jaramillo V., Fries A., Zeilinger J., Homeier J., Paladines-Benitez J., & Bendix J. 2018. Estimation of above ground biomass in a tropical mountain forest in southern Ecuador using airborne LiDAR data. Remote Sens. 10, 660. https://doi.org/10.3390/rs10050660.

Hauglin M., Rahlf J., Schumacher J., Astrup R., & Breidenbach J. 2021. Large scale mapping of forest attributes using heterogeneous sets of airborne laser scanning and National Forest Inventory data. Forest Ecosyst. 8, 65. https://doi.org/10.1186/s40663-021-00338-4.

Hill A., Buddenbaum H., & Mandallaz D. 2018. Combining canopy height and tree species map information for large-scale timber volume estimations under strong heterogeneity of auxiliary data and variable sample plot sizes. European J. Forest Res. 137, 489–505. https://doi.org/10.1007/s10342-018-1118-z.

Hollaus M., Wagner W., Schadauer K., Maier B., & Gabler K. 2009. Growing stock estimation for alpine forests in Austria: a robust lidar-based approach. Can. J. Forest Res. 39, 1387–1400. https://doi.org/10.1139/X09-042.

Hudak A.T., Crookston N.L., Evans J. S., Hall D.E., & Falkowski M.J. 2008. Nearest neighbour imputation of species-level, plot-scale forest structure attributes from LiDAR data. Remote Sens. Environ. 112(5), 2232–2245. https://doi.org/10.1016/j.rse.2007.10.009.

Ioki K., Imanishi J., Sasaki T., Morimoto Y., & Kitada K. 2010. Estimating stand volume in broad-leaved forest using discrete-return LiDAR: plot-based approach. Landscape Ecol. Eng. 6, 29–36. https://doi.org/10.1007/s11355-009-0077-4.

Jiang X., Li G., Lu D., Chen E., & Wei X. 2020. Stratification-based forest aboveground biomass estimation in a subtropical region using airborne Lidar data. Remote Sens. 12, 1101. https://doi.org/10.3390/rs12071101.

Keränen J., Maltamo M., & Packalen P. 2016. Effect of flying altitude, scanning angle and scanning mode on the accuracy of ALS based forest inventory. Int. J. Appl. Earth Obs. 52, 349–360. https://doi.org/10.1016/j.jag.2016.07.005.

Knapp N., Fischer R., Cazcarra-Bes V., & Huth A. 2020. Structure metrics to generalize biomass estimation from lidar across forest types from different continents. Remote Sens. Environ. 237, 111597. https://doi.org/10.1016/j.rse.2019.111597

Latifi H., Fassnacht F. E., Müller J., Tharani A., Dech S., & Heurich M. 2015. Forest inventories by LiDAR data: A comparison of single tree segmentation and metric-based methods for inventories of a heterogeneous temperate forest. Int. J. Appl. Earth. Obs. 42, 162–174. https://doi.org/10.1016/j.jag.2015.06.008

Laurin G.V., Puletti N., Chen Q., Corona P., Papale D., & Valentini R. 2016. Above ground biomass and tree species richness estimation with airborne lidar in tropical Ghana forests. Int. J. Appl. Earth Obs. 52, 371-379. https://doi.org/10.1016/j.jag.2016.07.008.

Leboeuf A., Riopel M., Munger D., Fradette M-S., & Bégin J. 2022. Modeling merchantable wood volume using airborne LiDAR metrics and historical forest inventory plots at a provincial scale. Forests, 13, 985. https://doi.org/10.3390/f13070985.

Lefsky M.A., Cohen W.B., Parker G.G., & Harding D.J. 2002. Lidar remote sensing for ecosystem studies. Bioscience, 52 (1), 19-30. https://doi.org.10.1641/0006-3568(2002)052.

Li C., Chen Z., Zhou X., Zhou M., & Li Z. 2023. Generalized models for subtropical forest inventory attribute estimations using a rule-based exhaustive combination approach with airborne LiDAR-derived metrics. Gisci. Rremote Sen. 60(1), 2194601. https://doi.org/10.1080/15481603.2023.2194601.

Liao Z., & Huang D. 1986. Forest inventory handbook of Guangxi, China. Unpublished work. Forestry department of Guangxi Zhuang autonomous region, Nanning, China. (in Chinese)

Liu H., Shen X., Cao L., Yun T., Zhang Z., Fu X., Chen X., & Liu F. 2021. Deep learning in forest structural parameter estimation using airborne LiDAR data. IEEE J-STARS. 14, 1603-1618. https://doi.org/10.1109/JSTARS.2020.3046053.

Luo S., Chen J. M., Wang C., Gonsamo A., Xi X., Lin Y., Qian M., Peng D., Nie S., & Qin, H. 2018. Comparative performances of airborne LiDAR height and intensity data for leaf area index estimation. IEEE J-STARS, 11(1), 300-310. https://doi.org/10.1109/JSTARS.2017.2765890.

Maltamo M., Bollandsas O.M., Gobakken T., & Nasset E. 2016. Large-scale prediction of aboveground biomass in heterogeneous mountain forests by means of airborne laser scanning. Can. J. For. Res. 46, 1138–1144. https://doi.org/10.1139/cjfr-2016-0086.

Maltamo M., Bollandsås O.M., Næsset E., Gobakken T., & Packalén P. 2011. Different plot selection strategies for field training data in ALS-assisted forest inventory. Forestry, 84(1), 23-31. https://doi.org/10.1093/forestry/cpq039.

Marczak P.T., Van Ewijk K.Y., Treitz P.M., Scott N.A., & Robinson D.C.E. 2020. Predicting carbon accumulation in temperate forests of Ontario, Canada using a LiDAR-Initialized growth-and-yield model. Remote Sens. 12, 201. https://doi.org/10.3390/rs12010201.

Matasci G., Hermosilla T., Wulder M.A., White J.C., Coops N.G., Hobart G.W., & Zald H.S.J. 2018. Large-area mapping of Canadian boreal forest cover, height, biomass and other structural attributes using Landsat composites and lidar plots. Remote Sens. Environ. 209, 90–106. https://doi.org/10.1016/j.rse.2017.12.020.

McRoberts R.E., Næsset E., Gobakken T., & Bollandsås O.M. 2015. Indirect and direct estimation of forest biomass change using forest inventory and airborne laser scanning data. Remote Sens. Environ. 164, 36–42. https://doi.org/10.1016/j.rse.2015.02.018.

Means J.E., Acker S.A., Fitt B.J., Renslow M., Emerson L., & Hendrix C.J. 2000. Predicting forest stand characteristics with airborne scanning lidar. Photogramm. Eng. Rem. S. 66(11), 1367-1371.

Montaghi A., Corona P., Dalponte M., Gianelle D., Chirici G., & Olsson H. 2013. Airborne laser scanning of forest resources: An overview of research in Italy as a commentary case study. Int. J. Appl. Earth Obs. 23, 288-300. https://doi.org/10.1016/j.jag.2012.10.002.

Næsset E. 2004. Practical large-scale forest stand inventory using a small-footprint airborne scanning laser. Scand. J. For. Res. 19, 164–179. https://doi.org/10.1080/02827580310019257.

Næsset E., Bollandsas O.M., Gobakken T., & Bollandsá O.M. 2005. Comparing regression methods in estimation of biophysical properties of forest stands from two different inventories using laser scanner data. Remote Sen. Environ. 94(4), 541–553. https://doi.org/10.1016/j.rse.2004.11.010.

Næsset E., & Økland T. 2002**.** Estimating tree height and tree crown properties using airborne scanning laser in a boreal nature reserve. Remote Sen. Environ. 79, 105–115. https://doi.org/10.1016/S0034-4257(01)00243-7.

Næsset. E. 2002. Predicting forest stand characteristics with airborne scanning laser using a practical two-stage procedure and field data. Remote Sens. Environ. 80, 88–99. https://doi.org/10.1016/S0034-4257(01)00290-5.

Nelson R.F., Hyde P., Johnson P., Emessiene B., Imhoff M.L., Campbell R., & Edwards W. 2007. Investigating RaDAR–LiDAR synergy in a North Carolina pine forest. Remote Sens. Environ. 110(1), 98–108. https://doi.org/10.1016/j.rse.2007.02.006.

Nelson R., Margolis H., Montesano P., Sun G., Cook B., Corp L., Andersen H-E., deJong B., Pellat F.P., Fickel T., Kauffman J., & Prisley S. 2017. Lidar-based estimates of aboveground biomass in the continental US and Mexico using ground, airborne, and satellite observations. Remote Sens. Environ. 188, 127–140. https://doi.org/10.1016/j.rse.2016.10.038.

Neto S.E.N., Paula A.D., Tagliaferre C., Barreto-Garcia P.A.B., & Júnior L.D. 2018. Performance assessment of methodologies for vertical stratification in native forest. Ciência florestal, 28(4), 1583−1591. https://doi.org/10.5902/1980509835106.

Nilsson M. 1996. Estimation of tree heights and stand volume using an airborne lidar system. Remote Sens. Environ. 56, 1-7. https://doi.org/10.1016/0034-4257(95)00224-3.

Nilsson M., Nordkvist K., Jonzén J., Lindgren N., Axensten P., Wallerman J., Egberth M., Larsson S., Liselott N., Eriksson J., & Olsson H. 2017. A nationwide forest attribute map of Sweden predicted using airborne laser scanning data and field data from the National Forest Inventory. Remote Sens. Environ. 194, 447–454. https://doi.org/10.1016/j.rse.2016.10.022.

Nord-Larsen T., & Schumacher J. 2012. Estimation of forest resources from a country wide laser scanning survey and national forest inventory data. Remote Sens. Environ. 119, 148–157. https://doi.org/10.1016/j.rse.2011.12.022.

Novo-Fernández A., Barrio-Anta M., Recondo C., Cámara-Obregón A., & López-Sánchez C.A. 2019. Integration of national forest inventory and nationwide airborne laser scanning data to improve forest yield predictions in North-Western Spain. Remote Sens. 11, 1693. https://doi.org/10.3390/rs11141693.

Palace M.W., Sullivan F.B., Ducey M.J., Treuhaft R.N., Herrick C., Shimbo J.Z., & Mota-E-Silva J. 2015. Estimating forest structure in a tropical forest using field measurements, a synthetic model and discrete return lidar data. Remote Sens. Environ. 161, 1–11. https://doi.org/10.1016/j.rse.2015.01.020

Penner M., Pitt D.G., & Woods M.E. 2013. Parametric vs. nonparametric LiDAR models for operational forest inventory in boreal Ontario. Can. J. Remote Sens. 39(5), 426–443. https://doi.org/ 10.5589/m13-049.

Silva C.A., Hudak A.T., Klauberg C., Vierling L.A., Gonzalez-Benecke C., de Padua Chaves Carvalho S., Rodriguez L.C. E., & Cardil A. 2017a. Combined effect of pulse density and grid cell size on predicting and mapping aboveground carbon in fast-growing Eucalyptus forest plantation using airborne LiDAR data. Carbon Bal. Manage. 12(1), 13. https://doi.org/10.1186/s13021-017-0081-1.

Silva C.A., Klauberg C., Hubdak A.T., Vierling L.A., Fennema S.J, & Corte P.D. 2017b. Modeling and mapping basal area of *Pinus taeda* L. plantation using airborne LiDAR data. An. Acad. Bras. Cienc. 89(3), 1895–1905. https://doi.org/10.1590/0001-3765201720160324.

Singh K.K., Chen G., McCarter J.B., Ross K., & Meentemeyer R.K. 2015. Effects of LiDAR point density and landscape context on estimates of urban forest biomass. ISPRS J. Photogramm. 101, 310–322. http://doi.org/10.1016/j.isprsjprs.2014.12.021.

Song Y., Imanishi J., Sasaki T., Ioki K., & Morimoto Y. 2016. Estimation of broad-leaved canopy growth in the urban forested area using multi-temporal airborne LiDAR datasets. Urban For. Urban Gree. 16, 142–149. https://doi.org/10.1016/j.ufug.2016.02.007

Tang H., Ganguly S., Zhang G., Hofton M.A., Nelson R.F., & Dubayah R. 2015. Characterizing leaf area (LAI) and vertical foliage profile (VFP) over the United States. Biogeoscience, 12, 13675-13710. https://doi.org.10.5194/bg-13-239-2016.

Treitz P., Lim K., Woods M., Pitt D., Nesbitt D., & Etheridge D. 2012. LiDAR sampling density for forest resource inventories in Ontario, Canada. Remote Sens. 4, 830-848. https://doi.org/10.3390/rs4040830.

van Leeuwen M., Hilker T., Coops N.C., Frazer G., Wulder M.A., Newnham G.J., & Culvenor D.S. 2011. Assessment of standing wood and fiber quality using ground and airborne laser scanning: A review. Forest Ecol. Manag. 261, 1467–1478. https://doi.org/10.1016/j.foreco.2011.01.032.

Viana H., Aranha J., Lopes D., & Cohen W.B. 2012. Estimation of crown biomass of *Pinus pinaster* stands and shrubland above-ground biomass using forest inventory data, remotely sensed imagery and spatial prediction models. Ecol. Mode. 226, 22–35. https://doi.org/10.1016/j.ecolmodel.2011.11.027.

Watt P., & Watt M.S. 2013. Development of a national model of Pinus radiate stand volume from lidar metrics for New Zealand. Int. J. Remote Sens. 34(15–16), 5892–5904. https://doi.org/10.1080/01431161.2013.798053.

White J. C., Tompalski P., Vastaranta M., Wulder M.A., Saarinen N., Stepper C., & Coops N.C. 2017. A model development and application guide for generating an enhanced forest inventory using airborne laser scanning data and an area-based approach. Natural Resources Canada, Canadian Forest Service, Canadian Wood Fibre Centre, Information Report FI-X-018. https://doi.org/10.13140/rg.2.2.26770.96964.

Woods M., Lim K., & Treitz P. 2008. Predicting forest stand variables from LiDAR data in the Great Lakes – St. Lawrence forest of Ontario. Forestry Chron. 84(6), 827-839. https://doi.org/10.5558/tfc84827-6.

Wulder M.A., White J.C., Nelson R.F., Næsset E., Ørka H.O., Coops N.C., Hilker T., Bater C.W., & Gobakken T. 2012. Lidar sampling for large-area forest characterization: A review. Remote Sen. Environ. 121, 196–209. https://doi.org/10.1016/j.rse.2012.02.001.

Yang T-R., Kershaw Jr J.A., & Ducey M. J. 2021. The development of allometric systems of equations for compatible area-based LiDAR-assisted estimation. Forestry, 94, 36–53. https://doi.org/10.1093/forestry/cpaa019.

Zhang Z., Cao L., She G. 2017. Estimating forest structural parameters using canopy metrics derived from airborne LiDAR data in subtropical forests. Remote Sens. 9, 940. https://doi.org/10.3390/rs9090940.

Zhao F., Guo Q., & Kelly M. 2012. Allometric equation choice impacts lidar-based forest biomass estimates: A case study from the Sierra National Forest, CA. Agr. Forest Meteorol. 165, 64–72. https://doi.org/10.1016/j.agrformet.2012.05.019.

Zhou X., Li C. 2023. Mapping the vertical forest structure in a large subtropical region using airborne LiDAR data. Ecol. Indic. 154, 110731. https://doi.org/10.1016/j.ecolind.2023.110731.

Zolkos S.G., Goetz S.J., & Dubayah R. 2013. A meta-analysis of terrestrial aboveground biomass estimation using lidar remote sensing. Remote Sens. Environ. 128, 289–298. https://doi.org/10.1016/j.rse.2012.10.017.